Journal of Medicinal Chemistry

Article

pubs.acs.org/jmc

Molecular Basis of Structure–Activity Relationships between Salphen Metal Complexes and Human Telomeric DNA Quadruplexes

Nancy H. Campbell,[†,§] Nurul H. Abd Karim,[‡,§] Gary N. Parkinson,[†] Mekala Gunaratnam,[†] Vanessa Petrucci,[†] Alan K. Todd,[†] Ramon Vilar,*[,‡] and Stephen Neidle*[,†]

[†]CRUK Biomolecular Structure Group, The School of Pharmacy, University of London, 29-29 Brunswick Square, London WC1N 1AX, U.K.

[‡]Department of Chemistry, Imperial College London, London SW7 2AZ, U.K.

Supporting Information

ABSTRACT: The first X-ray crystal structures of nickel(II) and copper(II) salphen metal complexes bound to a quadruplex DNA are presented. Two structures have been determined and show that these salphen–metal complexes bind to human telomeric quadruplexes by end-stacking, with the metal in each case almost in line with the potassium ion channel. Quadruplex and duplex DNA binding is presented for these two and other related salphen complexes, all with side-chains terminating in pyrrolidino end-groups and differing patterns of substitution on the salphen core. The crystal structures are able to provide rationalizations for the structure–activity data, and in particular for the superior quadruplex-binding of the nickel complexes compared to that of the copper-containing ones. The complexes show significant antiproliferative activity for the compounds in a panel of cancer cell lines. They also show telomerase inhibitory activity in the telomerase TRAP-LIG assay.

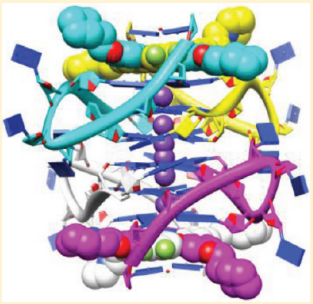

INTRODUCTION

The telomere is a nucleoprotein complex at the ends of eukaryotic chromosomes whose function is to protect the genome from unwanted recombination and damage events. It comprises noncoding DNA plus a complex array of telomere-specific proteins (the shelterin complex).[1] Telomere integrity can be maintained by the reverse transcriptase enzyme complex telomerase, which prevents critical shortening of telomeric DNA from occurring; in the absence of such a mechanism, telomeres progressively shorten during replication due to the inability of DNA polymerase to fully replicate telomeric DNA ends. Telomerase is expressed in ca. 80–85% of cancer cells (but not significantly in normal somatic cells) and plays a central role in cancer cell immortalization.[2] The natural substrate of telomerase is the 3′ single-stranded overhang of telomeric DNA, which is recognized by the RNA component of the telomerase complex. It has been shown that induction of higher-order structured DNA (i.e., quadruplex formation) in the guanine-rich single-stranded overhang can lead to inhibition of telomerase and, hence, to selective destabilization of telomere maintenance in cancer cells.[3] This concept has led to the design and development of a large and diverse superfamily of quadruplex-binding ligands based on a number of distinct heterocyclic frameworks.[4,5]

Some years ago, it was proposed that metal complexes coordinated to aromatic ligands could have the potential to be potent quadruplex DNA binders, and this was subsequently demonstrated to be the case with several examples.[6−9] In this concept, the metal center plays key structural, electronic, and electrostatic roles.[10] Structurally, it was envisaged that the metal can "organize" ligands into specific geometrical conformations ideally suited to $\pi-\pi$ stack onto a G-quartet (for example with square-planar and square-based pyramidal geometries). In addition, the metal center can also have an important electronic role of "pulling" electrons from coordinated aromatic ligands, making them more electron-deficient and therefore more likely to be involved in substantial $\pi-\pi$ interactions with G-quartets and nucleobases. Finally, the metal itself can also play an electrostatic role, being positively charged, and because it may be positioned at one end of the central ion channel in a quadruplex complex, it would thus occupy the place that a stabilizing potassium ion would normally occupy at the top of the G-quartet stack at the quadruplex core.

We have previously reported on several series of metal complexes that bind strongly to quadruplex DNA.[11−14] One of these series is based on metals (including nickel(II), copper(II), zinc(II), and vanadium(IV)) coordinated to salen and salphen tetradentate ligands (see Scheme 1).[6,15] Some of these complexes, in particular the square planar nickel(II) and copper(II) derivatives, have been shown to be excellent quadruplex DNA binders.[15] There has also been a report of platinum(II)–salphen derivatives as effective binders to *c-myc* quadruplex DNA.[16] However, remarkably little atomistic information concerning their exact mode of binding is known, beyond conjecture. The synthesis and initial biological evaluation of a series of nickel(II) and copper(II) salphen complexes is presented here together with spectroscopic studies to evaluate their affinity to human telomeric quadruplex DNA. We also present here the first X-ray crystal structures of two metal complexes from this series bound to a human telomeric quadruplex DNA, and derive some

Received: August 25, 2011
Published: November 24, 2011

dx.doi.org/10.1021/jm201140v | *J. Med. Chem.* 2012, 55, 209–222

Scheme 1. Reaction Scheme for the Synthesis of the Nickel(II) and Copper(II)−Salphen Complexes

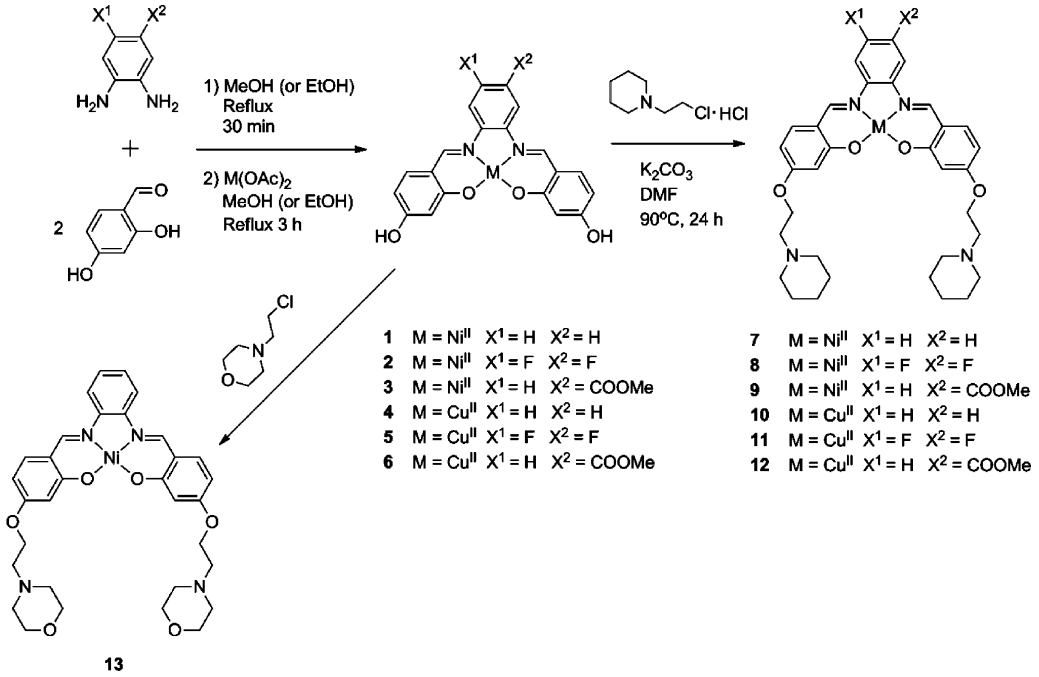

structure−activity relationships from them that have general applicability to other metal−ligand-quadruplex complexes.

RESULTS

Synthesis and Characterization of Metal Complexes. The metal salphene complexes **7**−**13** were prepared in two steps (see Scheme 1). First, unsubstituted salphen complexes **1**−**6** were synthesized by reacting the 2,4-dihydroxy-benzaldehyde with the corresponding diamine in the presence of either $Ni(OAc)_2$ or $Cu(OAc)_2$. The isolated products were then treated with chloro-ethyl-piperidine (or chloro-ethyl-morpholino for the synthesis of complex **13**) in the presence of a base to yield the disubstituted complexes, which were characterized by spectroscopic and analytic techniques (see Materials and Methods). It should be noted that we have previously reported the syntheses and DNA-binding properties (by FID, FRET and CD) of complexes **7**, **10** and **13**.[15]

FID, FRET, and UV−Vis Spectroscopic Determination of Affinities of Metal Complexes toward HTelo Quadruplex DNA. The DNA binding affinity of complexes **7**−**12** was first evaluated by the fluorescent intercalator displacement (FID) assay.[17] The poor solubility of the morpholino compound **13** precluded any binding studies apart from fluorescence resonance energy transfer (FRET) analyses (see below). As can be seen in Table 1, all the metal−salphen complexes examined here are effective binders to HTelo quadruplex DNA, with $^{50}DC_{Htelo}$ for all the complexes below the 0.5 μM "threshold" established in this technique for high-affinity quadruplex DNA binders.

Table 1. $^{HTelo}DC_{50}$ Values (μM) Determined Using the FID Assay and ΔT_m (°C) at 1 μM Determined by FRET for Complexes 7−12 (Values Are Average of Three Independent Measurements)

compd	$^{HTelo}DC_{50}$	ΔT_m (°C) at 1 μM
7	0.20	29.5 ± 0.4
8	0.33	26.1 ± 0.7
9	0.37	25.3 ± 0.7
10	0.29	24.0 ± 0.3
11	0.36	19.2 ± 1.1
12	0.26	19.7 ± 1.2

The affinity of the complexes for human telomeric (HTelo) quadruplex DNA was also investigated by FRET melting assays (see Table 1). The increase in melting temperature (ΔT_m) induced by complexes **7**−**12** at 1 μM concentration is in the range 19.2−29.5 °C. The ΔT_m value for the nickel(II) morpholino complex **13** is 4.6 °C less than the value for the corresponding piperidine complex **7**. All of the nickel(II) complexes induce higher DNA melting temperatures than the corresponding copper(II) ones. The nature of the substituents on the central ring plays only a minor role in defining the affinity of the complex (e.g., for the nickel(II) series ΔT_m values vary between 29.3 and 25.3 °C), although the unsubstituted complexes **7** and **10** induce higher melting temperatures of the quadruplex than the monoester and difluorine-substituted ones. UV−vis spectroscopic titrations were carried out in order to obtain the binding constants of the complexes toward HTelo quadruplex DNA and to gain insight into the binding mode of these complexes. The UV−vis spectra of all six salphen complexes showed similar patterns of behavior, with strong absorption in the region 300−320 nm (associated with intraligand π−π^* transitions) and a second one between 370 and 400 nm (which involves both the ligand and the metal center). Addition of increasing amounts of HTelo quadruplex DNA to the corresponding complexes resulted in considerable hypochromicity (between 12 and 26% for the band centered between 370 and 400 nm). In addition, a noticeable red-shift (ranging between 9 and 15 nm for the band centered at 370−400 nm) was also observed in all cases (see Figure 1a for an example). These spectral features are indicative of an end-stacking binding mode rather than groove binding. For comparison, we also studied the interactions between these six metal−salphen complexes and calf thymus (CT) DNA. Upon addition of increasing amounts of CT DNA to the complexes, hypochromicity was also

dx.doi.org/10.1021/jm201140v | J. Med. Chem. 2012, 55, 209−222

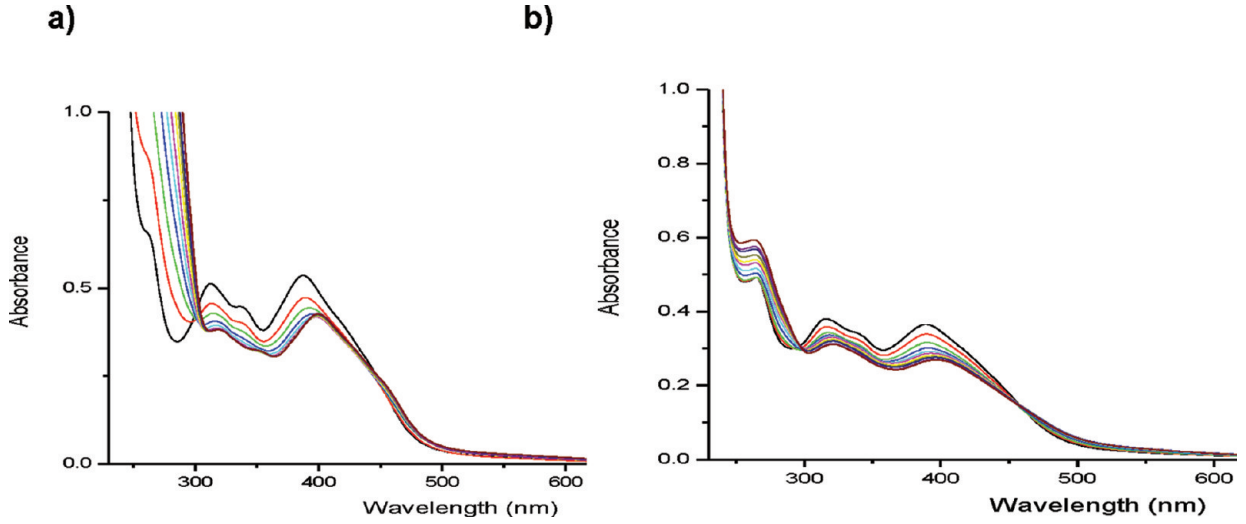

Figure 1. Representative examples of UV−vis titrations of metal−saphen complexes and DNA. The plots are for: (a) copper(II)−salphen complex **11** with HTelo (concentration of complex = 20 μM; increasing amounts of HTelo DNA were added between 0 and 0.5 equiv); (b) complex **11** with CT−DNA (concentration of complex = 20 μM; increasing amounts of HTelo DNA were added between 0 and 0.5 equiv).

observed (between 13 and 21%) but the red-shift was considerably smaller (under 4 nm in all cases; see Figure 1b), suggesting that these complexes are not good duplex DNA intercalators but may possibly act as duplex DNA groove binders.

The intrinsic binding affinities toward HTelo quadruplex and CT-DNA were determined by monitoring changes in complex absorption upon increasing DNA concentration. The results are summarized in Table 2. All the metal complexes were found to interact strongly with HTelo quadruplex DNA, with binding constants comparable to those of other metal complexes reported as high-affinity quadruplex DNA binders (in the 10^7−10^6 M^{-1} range).[14,18] In general the Ni complexes have higher quadruplex affinity than the Cu ones. The association constants between the complexes and CT-DNA are generally 10−50 fold lower than that for HTelo quadruplex DNA, with the exception of compound **7**, which is much more selective.

Table 2. Affinity Constants of Selected Compounds for HTelo and CT-DNA, Determined by UV−vis Spectroscopy

compd	$^{HTelo}K$ (M^{-1})	$^{CT\text{-}DNA}K$ (M^{-1})
7[a]	(1.27 ± 0.30) × 10^7	(8.96 ± 0.18) × 10^3
8[b]	(7.80 ± 0.16) × 10^6	(1.69 ± 0.39) × 10^4
9[c]	(8.51 ± 0.16) × 10^6	(4.24 ± 3.01) × 10^4
10[d]	(1.74 ± 0.31) × 10^5	(8.10 ± 0.81) × 10^4
11[e]	(1.72 ± 1.28) × 10^6	(2.92 ± 0.93) × 10^4
12[f]	(4.30 ± 1.84) × 10^6	(3.19 ± 1.36) × 10^4

[a]Absorption measured at 310 nm (HTelo) and at 367 nm (CT-DNA). [b]Absorption measured at 373 nm (HTelo and CT-DNA). [c]Absorption measured at 371 nm (Htelo and CT-DNA). [d]Absorption measured at 382 nm (HTelo and CT-DNA). [e]Absorption measured at 313 nm (HTelo and CT-DNA). [f]Absorption measured at 323 nm (HTelo and CT-DNA).

Circular Dichroism (CD) Spectroscopy. To assess the ability of these molecules to template the formation of quadruplex DNA, CD studies were carried out (except for complex **9**, which led to an overall decrease in intensity of the whole CD spectrum, likely to be associated with aggregation/precipitation at the concentrations needed for CD spectroscopic studies). Nonannealed HTelo DNA in the absence of K^+ (or added metal complex) showed the characteristic positive ellipticity at ca. 250 nm consistent with a singly stranded DNA sequence (see Figure 2). Upon addition of increasing amounts of the corresponding complexes, significant changes were observed in the CD spectra. With all the complexes, the signal centered at 250 nm decreased while the signals associated to the formation of quadruplex DNA increased. Interestingly, complexes **7** and **10** (which do not have substituents on the central ring) favored the formation of a parallel quadruplex DNA structure (with positive ellipticity centered at ca. 270 nm), while **8**, **11**, and **12** induced mainly the formation of an antiparallel quadruplex structure (with positive ellipticity centered at ca. 290 nm). An interesting feature of these CD spectra is the appearance of induced CD signals in the visible region. In the case of the copper complex **10**, signals at 385 nm (with negative ellipticity) and 450 nm (positive ellipticity) appear upon addition of increasing amounts of the complex. As with the analogous nickel complex **7**, one broad signal with positive ellipticity centered at ca. 430 nm was observed. The most intense induced CD signal (positive ellipticity at ca. 380 nm) was observed for the monosubstituted copper complex **12**. In contrast, the difluoro-substituted complexes **8** and **11** did not show significant induced CD signals. The induced CD signals for some of these complexes are further evidence that they bind to quadruplex DNA strongly because an achiral ligand (such as the compounds under study) can only give a CD signal when bound tightly to a chiral host (in this case quadruplex DNA).

Biological Evaluations. The antiproliferative properties of these compounds were evaluated in several cancer cell lines, and their activity in the TRAP-LIG[19] telomerase assay were determined (Tables 3 and 4). An insufficient amount of compound **10** was available for all of these determinations, so data on it is not presented; there is no reason to suggest that its behavior would be substantially different from the other compounds. All tested compounds show a high level of antiproliferative activity in every cancer cell line of this panel, albeit with only modest selectivity between cancer types. Only compounds **9** and **12**, containing a $-CO_2Me$ group, showed significant (though still modest) discrimination against the normal fibroblast cell line WI38, which does not express

dx.doi.org/10.1021/jm201140v | J. Med. Chem. 2012, 55, 209−222

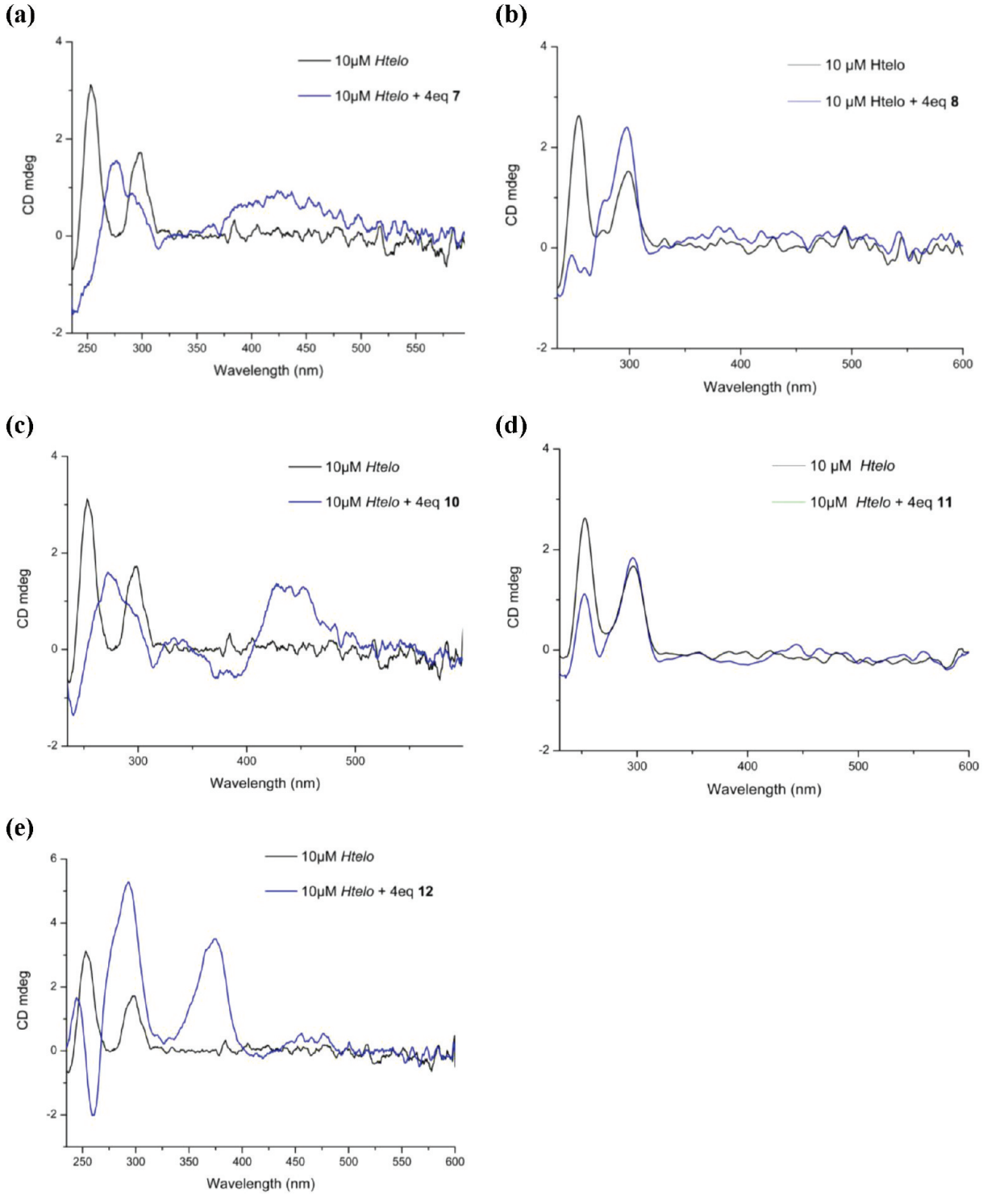

Figure 2. CD spectra of nonannealed HTelo DNA in the absence of K^+ upon addition of: (a) complex **7**; (b) complex **8**; (c) complex **10**; (d) complex **11**; (e) complex **12**. The spectra showed the disapearance of the 250 nm signal (single-stranded DNA) and the appearance of a signal with positive ellipticity at either 270 nm (parallel structure) or 290 nm (antiparallel structure). In some cases, induced CD signals in the region 350−500 nm are also observed.

telomerase. The two Cu-containing complexes have greater activity in the telomerase inhibition assay than the Ni ones, although the small number of compounds examined must preclude any firm conclusions. The morpholino compound **13** does not show activity in the MCF7, A549, or WI38 cell lines; in common with the other compounds it did appear to be taken up into cells, as qualitatively judged by color changes in treated cells, and further studies on it were discontinued.

Crystal Structures of Quadruplexes with Bound Metal Complexes 8 and 11. With the aim of unambiguously establishing the mode of quadruplex binding for these metal−salphen complexes, a series of crystallization trials between the complexes and a number of quadruplex DNA sequences were carried out. From these, two systems yielded single crystals that were suitable for single crystal X-ray analyses. These are the first reported 3-D molecular structures for any metal complexes

dx.doi.org/10.1021/jm201140v | J. Med. Chem. 2012, 55, 209−222

Table 3. Short-Term Growth Inhibition, as Measured by the SRB Method, for Selected Compounds, with IC_{50} Values in μM, for a Panel of Cell Lines[a]

	IC_{50}						
compd	MCF7	A549	RCC4	RCC4-VHL	786−0	Mia-PaCa-2	WI38
7	2.3	2.3	2.3	2.3	2.3	2.3	2.4
8	2.4	0.8	3.2	14.9	3.5	6.4	6.0
9	2.3	2.3	2.3	4.9	6.6	4.8	10.6
11	ND	2.2	2.3	2.3	2.3	2.3	5.8
12	2.3	2.3	2.3	2.3p	6.1	2.3	11.2

[a]Cancer cell lines are: MCF7 (breast), A549 (lung), RCC4 (renal), RCC4-VHL (renal), 786-0 (renal), MiaPaCa-2 (pancreatic). WI38 is a normal human fibroblast cell line. ND: not determined. Esds average ±0.2 μM.

bound to a G-quadruplex DNA. The structures involving complexes **8** and **11** were solved to a resolution of 2.4 Å using the multiwavelength anomalous dispersion (MAD) phasing method combined with molecular replacement (MR). Both structures comprise a bimolecular quadruplex that has been formed by the sequence d(AGGGT^{Br}UAGGGTT), where ^{Br}U is 5-bromo-2′-deoxyuridine-5′-monophosphate, together with a bound complex, the square-planar nickel(II) or copper(II) complexes **8** or **11** (Figure 3a−d). The **11**-quadruplex crystal structure was solved first and then was used to solve the **8**-quadruplex structure by MR methods. The final refined structures for the **8**- and **11**-quadruplex complexes are identical in terms of overall quadruplex topology, detailed conformation, and position of the metal complexes.

Both structures have a parallel bimolecular quadruplex topology based on a core of three stacked G-quartets (Figure 3a,b), with the quadruplexes having 2-fold crystallographic symmetry. The "biological" unit in each case comprises two quadruplexes, also related by 2-fold-symmetry, that each interact by $\pi-\pi$ stacking on their 5′ and 3′ end G-quartet faces. These form the basis of two-dimensional infinite parallel columns throughout the crystal, while the TTA loops from each quadruplex, extending laterally and interacting with their symmetry-related equivalents, provide sidelong connections that add overall stability to the crystal arrangement. Large solvent channels intersperse the columns (Figure 3a). The TTA loops adopt a propeller conformation (Figure 3b). The 5′ end G-quartet face of each quadruplex stacks directly onto the 5′ end G-quartet face of a symmetry-related quadruplex, while the 3′ end G-quartet face interacts, albeit indirectly, with its equivalent in another quadruplex. The stability of the arrangement at the 5′-5′ end G-quartet faces is further enhanced by the role of two adenines; one adenine is a flanking nucleotide belonging to the 5′ end of the DNA sequence and the other is a loop nucleotide belonging to the TTA loop. Each of these adenine nucleotides from one quadruplex interacts by stacking with its equivalent from a neighboring quadruplex (Figure 3b).

The stacking arrangement at the 3′-3′ end G-quartet faces in the **8** and **11**-containing structures is more complicated in that in each the complex stacks directly onto the 3′ end G-quartet face on one side and onto a pair of water-bridged thymine bases on the other (Figures 3c,d, 4a−d); these thymines are the 3′-terminal residues on each strand. Each thymine base pair belonging to one quadruplex then stacks onto their equivalent from a neighboring quadruplex one unit cell along (Figures 3c,d).

Potassium ions have been located at positions between successive G-quartets within an individual quadruplex, such that they coordinate the O6 atoms of guanine bases in a bipyramidal antiprismatic arrangement. Each metal ion in both salphen complexes, although not precisely in line with the set of potassium ions in the central ion channel of each quadruplex, is only 0.1−0.2 Å away from the center of the ion channel (Figure 5c). There is thus an almost continuous column of metal ions in each channel of the two cationic side-chain complexes, with the pattern interrupted only by a water molecule at the center of the thymine−thymine base pair that caps each bound ligand molecule.

Table 4. Telomerase Inhibition, in μM, Determined by the TRAP-LIG Method[a]

compd	$^{tel}EC_{50}$
7	11.7
8	19.2
9	5.3
11	3.6
12	4.8

[a]Esds average ±1.0 μM.

Both metal complexes, even though they stack directly onto the 3′ end G-quartet face (Figure 5c), are disordered along the 2-fold axis that passes through the central potassium ion channel. The metal complexes are significantly nonplanar (as discussed further below), and are slightly symmetrically bent into a butterfly like conformation (Table 6, Figure 5a). For both complexes **8** and **11**, electron density for each individual ligand molecule is well-defined except at the terminus of one side-chain (Figure 4a,b). Both disordered half-occupancy complexes are shown in parts a and b of Figure 4. The aromatic core of each complex is positioned slightly asymmetrically onto the 3′ end G-quartet, stacking mainly over the pyrimidine ring of one guanine on one side and onto one of the thymines belonging to the water-bridged thymine−thymine pair. The overlap ensures that the two fluorine atoms in each central ring of the complexes are oriented close to an imidazole group of one guanine base in the terminal G-quartet (Figure 5c), although the extent of overlap is not optimal.

The two side-chains of each complex **8** and **11** are not equivalent with respect to their position and interaction with the quadruplex. One side-chain extends downward toward a quadruplex groove, embedding its terminal piperidine ring deep within it. This ring also interacts with the quadruplex backbone through a weak water hydrogen-bonding bridge involving the ring nitrogen atom in the piperidine ring (3.3 Å distance), which in turn forms another hydrogen bond with a phosphate oxygen atom from the quadruplex backbone (2.9 Å) (Figure 6a). The other side-chain extends toward the TTA loop but does not form direct interactions with it (Figure 6b).

There is one crystallographically independent TTA loop in each quadruplex structure. Its conformation is distinct from the

dx.doi.org/10.1021/jm201140v | J. Med. Chem. 2012, 55, 209−222

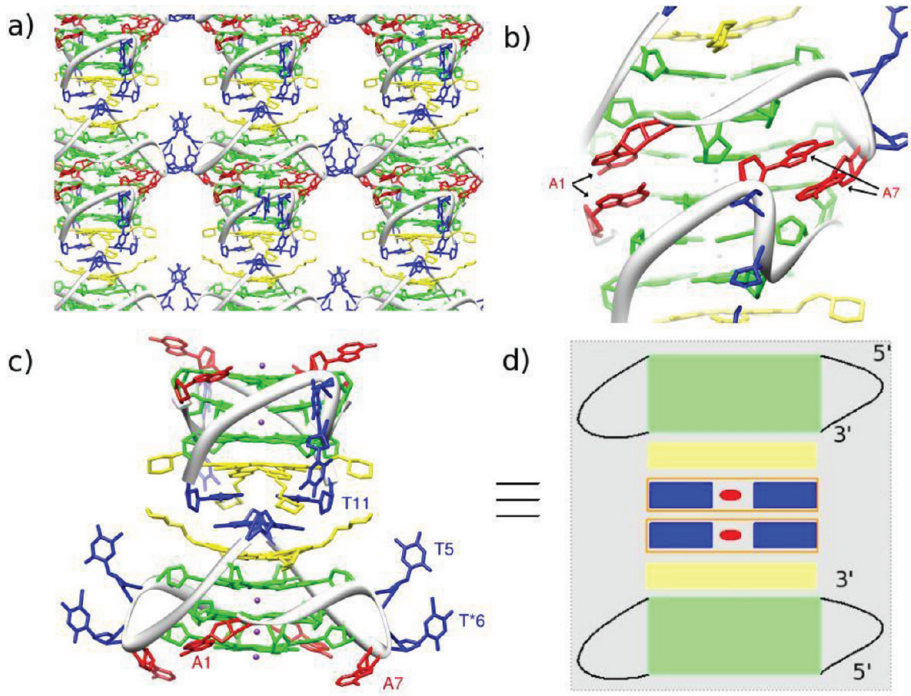

Figure 3. (a) Quadruplex units in the crystal. (b) Two quadruplexes interact at their 5′ end G-quartet faces showing the adenine pairs A1·A1 and A7·A7. (c) Two quadruplexes interact at their 3′ end G-quartet faces separated by a ligand and a pair of water-bridged thymine bases. (d) Schematic showing the arrangement at the 3′ end G-quartet faces where the ligand (yellow) stacks between a quadruplex (green) and a pair of water (red) bridged thymines (blue). Ligand is shown in yellow, guanines in green, adenine in red, and thymines in blue.

TTA loops observed in either native or other ligand-bound human telomeric quadruplexes[20] (Figure 5b). This further emphasizes the flexibility of the TTA loop and its ability to take up whatever conformation optimizes ligand binding (and to some extent crystal contacts). The electron density clearly reveals the loops extending laterally in a propeller conformation where the nucleotides interact with their equivalents from neighboring quadruplexes (Supporting Information Figure S1a–d). The lateral interactions of the two thymine nucleotides T5 and ^{Br}U6 contributes to sidelong stability in the crystal lattice (Supporting Information Figure S1a). On the other hand, the adenine nucleotide A7 contributes to longitudinal crystal stability by folding back into the adjacent quadruplex groove and stacking onto its equivalent from an adjacent quadruplex (Figure 3b). The first thymine T5 stacks onto its equivalent from a neighboring quadruplex (Supporting Information Figure S1b). The second (modified) thymine, ^{Br}U6, extends toward a neighboring T*6 and form electrostatic interactions (Supporting Information Figure S1c). Also, N3 in this thymine forms a hydrogen bond (2.7 Å) with an oxygen atom belonging to the DNA backbone of a neighboring quadruplex (Supporting Information Figure S1a).

DISCUSSION

The two crystal structures presented here show that salphen–metal complexes bind to human telomeric quadruplexes by end-stacking, with the metal in each case almost in line with the potassium ion channel. However, by contrast with alkali metal ions held within the quadruplex core, neither the Ni^{2+} nor the Cu^{2+} ions are coordinated to the O6 guanine substituent atoms (distances of 3.8 and 4.1 Å compared to K^+–O6 distances here of 2.5–2.9 Å). This is unsurprising because the ions in both complexes are held in the stacking plane above the terminal G-quartet. Thus there is no structural reason for the Ni^{2+} and Cu^{2+} ions to be precisely in line with the K^+ ion channel, and their observed positions probably reflect the optimum positions dictated by the stacking interactions. Comparison with the G-quartet stacking found (Figure 5d) in the telomeric quadruplex cocrystal structure with the acridine compound BRACO-19[20b] shows some similarities in that in both instances there is guanine overlap involving two phenyl rings; in the case of BRACO-19, it is the two outer phenyl rings of the acridine moiety. It is also striking that in both instances a central coordinating atom is positioned approximately above the central cationic channel. In the BRACO-19 complex, this is a water molecule that bridges between the ligand and an in-plane thymine group. In the present structures, it is the Ni^{2+} or Cu^{2+} coordinating ion (Figure 5e). It is also apparent that one piperidine ring of the salphen complex populates the same groove as one of the pyrrolidine rings of BRACO-19, and one piperidine ring of the second half-occupancy salphen complex is in the same groove as the *N*-methyl anilino substituent of BRACO-19, which is kept in place by a stacked thymine group from a TTA quadruplex loop. This suggests that an asymmetric salphen complex with an analogous anilino-type group could in this way have enhanced binding and selectivity to a human telomeric quadruplex.

The cationic side-chains in the **8**- and **11**-quadruplex crystal structures are observed to reside in the quadruplex grooves, in accord with other ligand complexes,[20] and the sole (water-mediated contact) with phosphate groups involves one of the charged nitrogen atoms of one piperidine ring. This suggests that extension of the side-chains may lead to enhanced phosphate contacts and superior affinity, albeit at the cost of higher molecular weight and possible greater hydrophobicity.

Examination of the crystal structures shows that a single substituent on the central phenyl ring of the salphen moiety has adequate space around it and does not interact with the quadruplex; this is in accord with the binding data, which shows

dx.doi.org/10.1021/jm201140v | J. Med. Chem. 2012, 55, 209–222

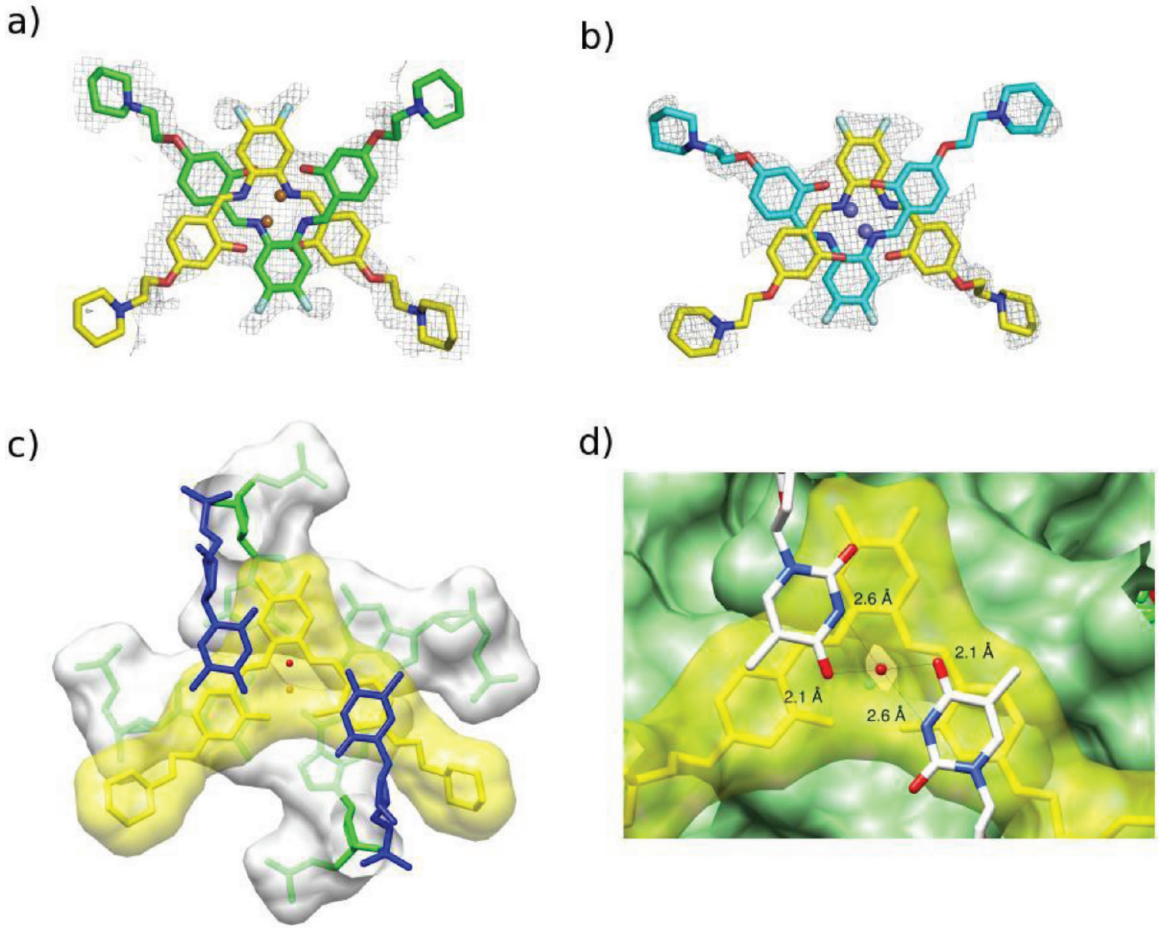

Figure 4. CD spectra of non-annealed HTelo DNA in the absence of K^+ upon addition of: (a) complex **7**; (b) complex **8**; (c) complex **10**; (d) complex **11**; (e) complex **12**. The spectra show the disappearance of the 250 nm signal (single stranded DNA) and the appearance of a signal with positive ellipticity at either 270 nm (parallel structure) or 290 nm (anti-parallel structure). In some cases, induced CD signals in the region 350−500 nm are also observed.

that complexes **9** and **12**, each with a single $-CO_2Me$ group, bind as well as the difluoro complexes **8** and **11**. It is at first sight surprising that the difluoro complexes are slightly less effective quadruplex binders than the native complexes **7** and **10** because the electronegativity of the fluorine atoms would be expected to enhance stacking interactions for the central phenyl ring of the complexes. The crystal structures are able to rationalize this and show that this ring is barely overlapping with the adjacent guanine. Increased overlap is implausible given that this would result in highly asymmetric binding with the metal ions displaced from the axis of the channel. Also, one fluoro substituent is proximal to an electronegative O6 guanine atom (Figure 5c). The electrostatic repulsions of these two atoms will contribute to a decrease in binding ability.

The largest differences in binding overall are between the Ni^{2+} and Cu^{2+} complexes (Tables 1, 2), with the former binding more strongly and stabilizing the quadruplex to a greater extent. The crystal structures show small but significant differences that provide a molecular explanation for the binding data. Both of the two complexes have butterfly like conformations, whose bending when bound to the quadruplex is reduced compared to that observed in the native complexes. However, the bending of the Ni^{2+} complex is less than that of the Cu^{2+} one. Figure 5a shows that the effect of this difference in bending is to change the degree to which stacking of the phenyl rings can occur, with differences in stacking distances of 0.2−0.3 Å. These differences are sufficient to result in distinct stacking energies and binding affinities.

It is notable that the potency of in vitro telomerase inhibition (Table 4) does not correlate well with the rank order of quadruplex affinities, suggesting that telomerase inhibition by these complexes may involve, for example, direct complex binding at the active site as well as the more indirect quadruplex telomeric DNA substrate. The pattern of cell growth inhibition in the cancer cell line panel (Table 3) does not correlate well with the FRET data. Overall the best compound in the series, taking activity in the panel, selectivity for the cancer lines, and telomerase inhibitory activity into account, is compound **12**. We conclude that telomeric quadruplex binding and telomerase inhibitory activity are both necessary for effective inhibition of cell proliferation but probably by themselves insufficient. We therefore cannot discount the possibility that the cellular activity of these compounds is due to them also acting at other targets such as genomic quadruplex sites such as promoter quadruplexes,[21] as recently reported for some Schiff base complexes.[16] This will be examined in subsequent studies by us.

The formation of a pseudolateral loop/cap over the complexes by a terminal thymine residue has not been observed previously in telomeric quadruplex−small molecule complexes. It resembles the lateral loop observed to enclose acridine derivatives in a series of complexes with a bimolecular quadruplex from the

dx.doi.org/10.1021/jm201140v | J. Med. Chem. 2012, 55, 209−222

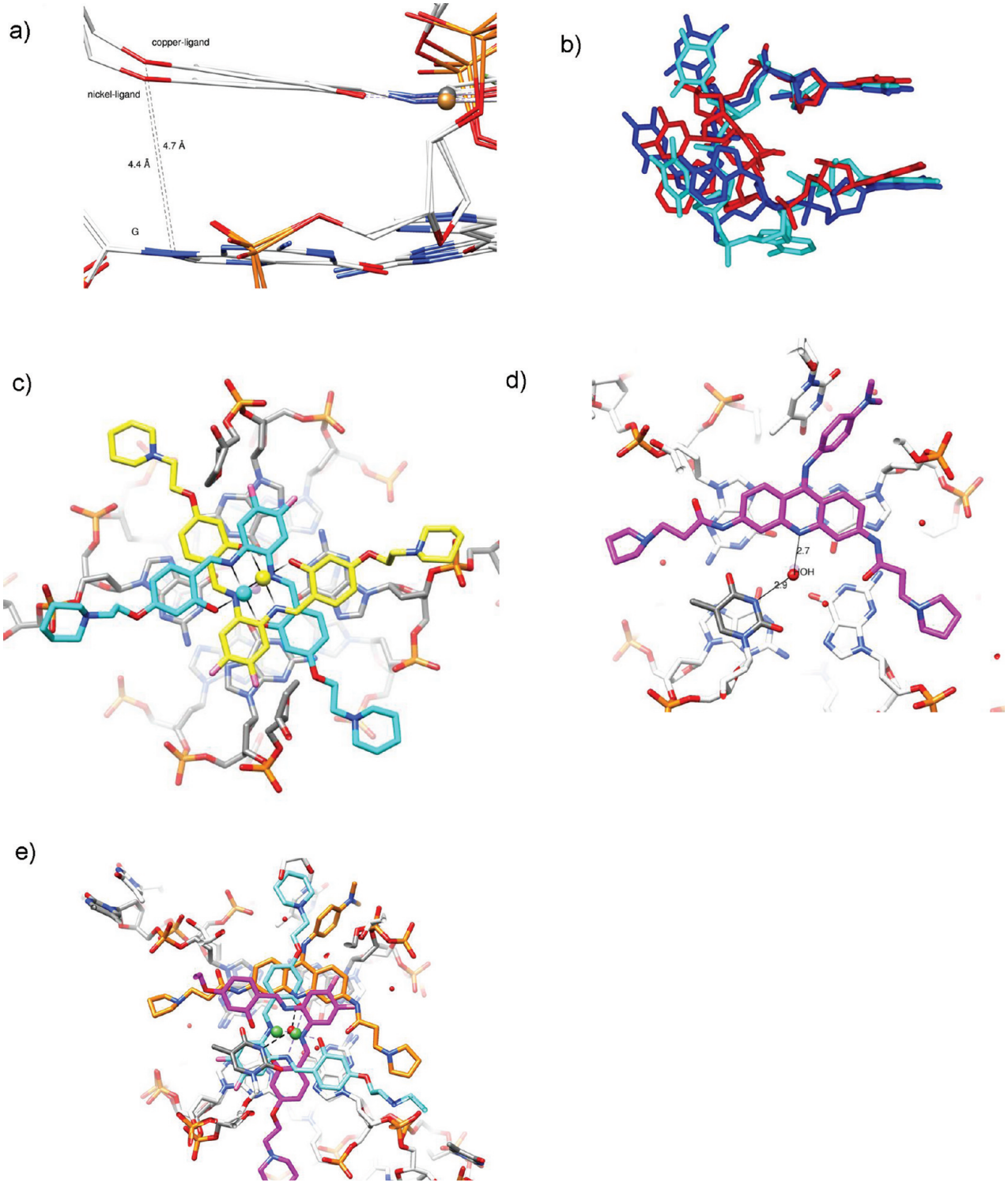

Figure 5. (a) Detailed view of the two superimposed structures and projected along the plane of the complexes, comparing the stacking interaction of the two complexes with the adjacent G-quartet. Part of each ligand is shown at the top of the figure. The distances between the ether oxygen atom in each complex and the stacked guanine are shown, highlighting the differences in buckle between the Ni^{2+} and Cu^{2+} complexes when bound. (b) Superposition of three TTA loops in three human telomeric quadruplexes: the native is colored in red, the BRACO-19 complex is in dark blue, and the present Ni/Cu complex is in cyan. (c) View showing overlap of the two disordered molecules in the Ni^{2+} complex with the adjacent G-quartet. Each Ni^{2+} ion is shown as a sphere in the same color as its salphen complex; coordination to the salphen molecules is also shown. The column of K^+ ions is just visible in the center of the figure. (d) View of the BRACO-19-telomeric quadruplex complex[20b] (PDB ID 3CE5), projected onto the G-quartet plane. The BRACO-19 molecule (in mauve) is shown together with an in-plane thymine group (with carbon atoms colored gray) and the water molecule bridging between these two groups. (e) View of the BRACO-19 and Ni−salphen structures, with the stacked G-quartets (at the rear of the view) overlaid on one another. The BRACO-19 molecule is shown in orange, and the two salphen complexes are in blue and mauve. The two central Ni^{2+} ions are shown as green spheres, close to the water molecule in the center of the BRACO-19 structure.

dx.doi.org/10.1021/jm201140v | *J. Med. Chem.* 2012, 55, 209−222

Table 5. Crystallographic Data[a]

	PDB ID	
	3QSC	3QSF
ligand	**8**	**11**
Data Collection		
total number of reflns	7709	6662
no. of unique reflns	2020	1888
space group	*C*222	*C*222
cell dimensions: a, b and c (Å)	43.75, 54.79, 33.43	44.02, 54.91, 33.69
maximum resolution (Å)	2.25	2.31
overall		
R_{merge}	0.034	0.053
I/σ	24.9	15.1
completeness (%)	98.2	97.4
redundancy	3.8	3.5
highest resolution shell		
R_{merge}	0.095	0.153
I/σ	8.5	5.7
completeness (%)	91.5	89.8
redundancy	2.6	2.7
Refinement		
resolution range used in refinement (Å)	15.0−2.4	15.0−2.4
no. of unique reflns used in refinement	1610	1607
completeness (%)	99.1	97.0
R_{factor} (%)	21.3	23.6
R_{free} (%)	23.4	32.1
no. of G-quadruplexes per asymmetric unit	1/2	1/2
no. of ligands per asymmetric unit	1	1
no. of asymmetric units per unit cell	8	8
no. of atoms	307	306
no. of DNA atoms	231	231
no. of ligand atoms	45	45
no. of potassium ions	3	3
no. of water molecules	29	28

[a]One crystal was used for each native data collection and structure determination.

organism *Oxytricha nova*.[22] We note that a TTA loop in such a position in a longer telomeric DNA sequence could conceivably also form such a flap.

SUMMARY: IMPLICATIONS FOR QUADRUPLEX LIGAND DESIGN

(1) Metal-salphen complexes can bind effectively to human telomeric (and probably other) quadruplexes by direct end-stacking. Planar groups that coordinate the metal ion can also play a stabilizing role.
(2) The nature of the metal ion is important because even small changes in ionic radius have an effect on the ability of the complex to bind effectively to quadruplexes.
(3) The nature and size of the side-chains is important for quadruplex binding. The crystal-structure data suggests that compound **8**, for example, may be substantially improved upon by lengthening the side-chains
(4) There is substantial unused space around some parts of the stacked metal complex that in the present structures are "inert" and thus capable of functionalization without affecting quadruplex binding. These can be exploited in order to improve pharmacological properties such as uptake, metabolism and distribution.

MATERIALS AND METHODS

General Procedures for Characterization of Compounds. ^{1}H NMR and ^{13}C NMR spectra were recorded on either a Bruker Avance 400 MHz Ultrashield NMR spectrometer or a Bruker Avance 500 MHz NMR spectrometer. Mass spectrometric analysis was performed under ESI+ condition on a LCT Premier mass spectrophotometer. UV−vis spectra were collected on a Perkin-Elmer UV−vis spectrophotometer. IR spectra were recorded on a Perkin-Elmer Spectrum 100 FT-IR spectrometer. All chemical were purchased from Sigma-Aldrich, BDH, or Apollo Scientific and used without further purification. Compounds **1**, **4**, **7**, **10**, and **13** were prepared as previously reported.[15]

N,N′-Bis-4-(hydroxysalicylidene)-4,5-difluorophenylenediamine-nickel(II) (**2**). 1,2-Diamino-4,5-difluorobenzene (0.360 g, 2.5 mmol) and 2,4-dihydroxybenzaldehyde (0.699 g, 5.0 mmol) were dissolved in methanol (50 mL) and heated for 30 min at reflux. $Ni(OAc)_2{\cdot}4H_2O$ (1.244 g, 5.0 mmol) was then added and a brown solid precipitated immediately. The reaction was refluxed for a further 3 h. After this time, the reaction mixture was cooled to room temperature. The dark-brown precipitate formed was filtered and washed with methanol (100 mL), diethyl ether (50 mL), and water (50 mL) to afford **2** as a dark-brown solid. Yield: 0.41 g, 37%. ^{1}H NMR (DMSO-d_6, 400 MHz,): δ 6.20 (d, $^4J_{HH}$ = 2 Hz, 2H, ArH), 6.23 (dd, 2H, $^3J_{HH}$ = 8.4 Hz, $^4J_{HH}$ = 2 Hz, ArH), 7.32 (d, $^3J_{HH}$ = 8.4 Hz, 2H, ArH), 8.15 (t, $^3J_{HF}$ = 10.0 Hz, 2H, ArH) 8.42 (s, 2H, CH═N−), 10.28 (s, 2H, −OH) . ^{13}C NMR (400 MHz, DMSO-d_6) δ 103.4, 103.9 ($^2J_{CF}$ = 23.9 Hz, $^3J_{CF}$ = 12.1 Hz), 108.1, 114.4, 135.7, 138.7, 146.5, 148.5, 154.8, 165.9 ($^1J_{CF}$= 257 Hz). IR (cm^{-1}): 1162 (C−F), 1589 (C═N), 1162 (C−OH), 1436 (C═C), 1371 (C═C), 1123 (C═C). ESI-MS (M+) *m*/*z* calcd for $C_{20}H_{12}N_2F_2NiO_4$, 441.0 amu; found, 441.0 amu. Anal. Calcd for $C_{20}H_{12}N_2F_2NiO_4{\cdot}0.5CH_3OH$: C, 53.87; H, 3.09; N, 6.13. Found: C, 54.19; H, 3.14; N, 5.47.

N,N′-Bis[4-[[1-(2-ethyl)piperidine]oxy]salicylidene]-4,5-difluoro-1,2-phenylenediamine-nickel(II) (**8**). A suspension of **2** (0.132 g, 0.3 mmol), 1-(2-chloroethyl)piperidine hydrochloride (0.276 g, 1.5 mmol), and K_2CO_3 (0.332 g, 2.4 mmol) in dry DMF (30 mL) was heated at 90 °C overnight. After this time, the excess salts were removed by filtration and the DMF evaporated under reduced pressure. The resulting dark-red solid was recrystallized with DCM:*n*-pentane (1:5) to give **8** as an orange−red solid. Yield: 0.17 g, 40%. ^{1}H NMR (400 MHz,$CDCl_3$: δ 1.47−1.48 (br m, 4H, piperidine-H), 1.61−1.66 (m, 8H, piperidine-H), 2.52 (br, 8H, piperidine), 2.8 (t, $^3J_{HH}$ = 6.0 Hz, 4H, $-CH_2N$,), 4.13 (t, $^3J_{HH}$ = 6.0 Hz, 4H, $-CH_2O-$), 6.38 (dd, $^3J_{HH}$ = 8.8, $^4J_{HH}$ = 2 Hz, 2H, ArH), 6.62 (d, $^4J_{HH}$ = 2 Hz, 2H, ArH), 7.20 (d, $^3J_{HH}$ = 8.8 Hz, 2H, ArH), 7.46 (t, $^3J_{HF}$ = 8.8 Hz, 2H, ArH), 7.84 (s, 2H, −CH═N−). ^{13}C NMR (400 MHz, $CDCl_3$): δ 24.2, 25.9, 55.0, 57.6, 66.1, 102.4, 103.0, 104.1, 109.7, 114.5, 134.2, 152.3, 167.0 ($^1J_{CF}$ = 300 Hz) . IR (cm^{-1}): 1171 (C−F), 1587 (C═N), 1147 (C−O), 2932 (CH_2−), 2855 (CH−O), 1435 (C═C), 1123 (C═C), 1369 (C═C). UV−vis ($CHCl_3$): λ_{max} = 392 nm (ε = 6.77 × 10^4 cm^{-1} M^{-1}), 312 nm (ε = 4.88 × 10^4 cm^{-1} M^{-1}). ESI-MS (M+) *m*/*z* calcd for $C_{34}H_{38}F_2N_4NiO_4$ (M^+), 663.38; found, 663. Anal. Calcd for $C_{34}H_{38}F_2N_4NiO_4$: C, 61.56; H, 5.77; N, 8.45. Found: C, 61.58; H, 5.73; N, 8.47.

N,N′-Bis-4-(hydroxysalicylidene)4-methylesterphenylenediamine-nickel(II) (**3**). Methyl 3,4-diaminobenzoate (0.441 g, 2.5 mmol) and 2,4-dihydroxybenzaldehyde (0.699 g, 5.0 mmol) were dissolved in methanol (50 mL) and heated for 30 min at reflux. $Ni(OAc)_2{\cdot}4H_2O$ (1.244 g, 5.0 mmol) was then added to the reaction mixture, and a red solid precipitated immediately. The reaction was refluxed for a further 3 h. After this time, the reaction mixture was cooled to room temperature. A red precipitate formed, which was filtered and washed with methanol (100 mL), diethyl ether (50 mL), and water (50 mL) to afford **3** as an orange−red solid. Yield: 0.57 g, 49%. ^{1}H NMR (400 MHz, DMSO-d_6): δ 3.92 (s, 3H, CH_3COO-), 6.22 (br s, 2H, ArH), 6.26 (dd, $^3J_{HH}$ = 8.8 Hz, $^4J_{HH}$ = 2.1 Hz, 2H, ArH), 7.42 (d, $^3J_{HH}$ = 8.8 Hz, 1H, ArH,), 7.53 (d, $^3J_{HH}$ = 8.8 Hz, 1H, ArH,), 7.70 (dd, $^3J_{HH}$ = 8.8, $^4J_{HH}$ = 1.2 Hz, 1H, ArH), 8.11 (d, $^3J_{HH}$ = 8.8 Hz, 1H, ArH), 8.53 (d, $^4J_{HH}$ = 1.2 Hz, 1H, ArH), 8.62 (s, 1H, −CH═N), 8.69 (s, 1H, −CH═N), 10.35 (s, 1H, −OH). ^{13}C NMR (DMSO-d_6, 400 MHz) δ 52.8,

dx.doi.org/10.1021/jm201140v | J. Med. Chem. 2012, 55, 209−222

Table 6. Torsion Angles (deg) for the CSD Entry LOQKUY, Together with Values for Complexes 8 and 11 as Bound to the Human Telomeric Quadruplex

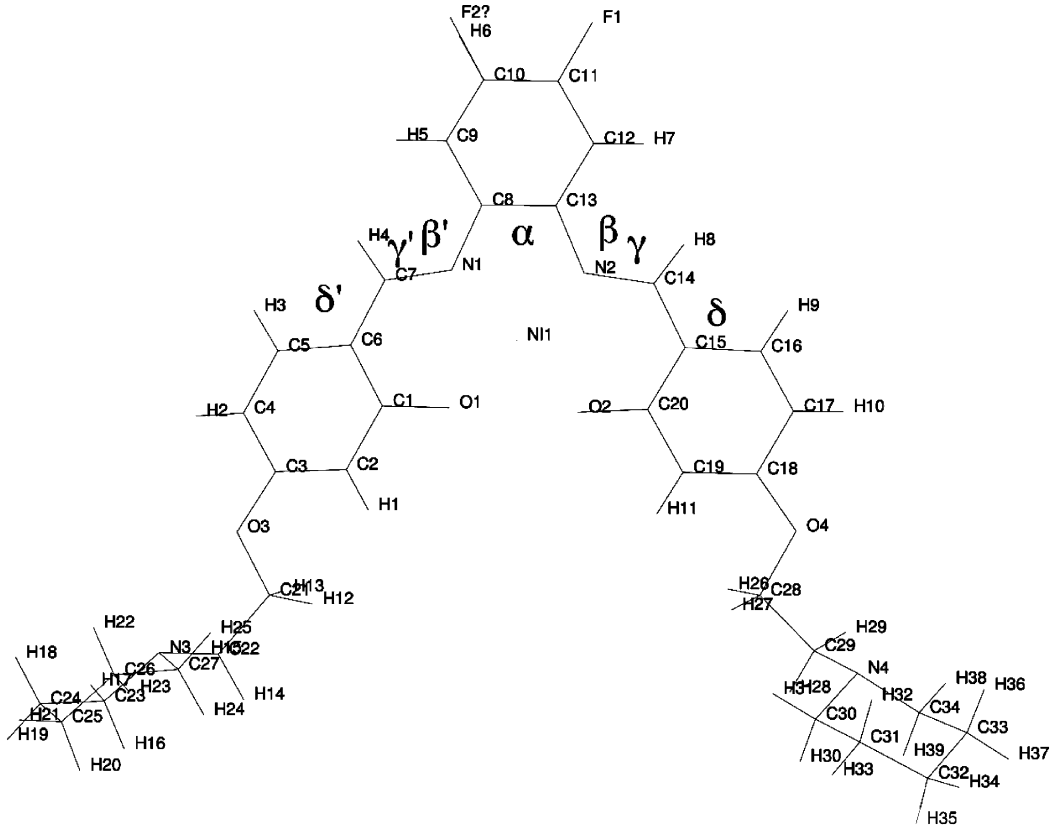

ligand	α	β	β'	γ	γ'	δ	δ'
LOQKUY	3	−177	167	177	−180	0	−6
complex **8**	1	−168	163	175	−175	−6	8
complex **11**	1	−168	169	175	−175	−5	5

103.8, 103.9, 108.4, 109.0, 115.1, 115.0, 115.9, 116.7, 127.3, 127.4, 136.7, 142.9, 146.7, 155.2, 155.5, 165.1, 165.5, 166.0, 167.9, 168.5. IR (cm^{-1}): 1687 (C═O), 1234 (HO−C═O), 1608 (C═N), 1124 (C−OH), 1487 (C═C), 1502 (C═C). ESI-MS (M+) m/z calcd for $C_{22}H_{16}NiN_2O_6$ (M+), 463.1 amu; found, 463.0. Anal. Calcd for $C_{22}H_{16}NiN_2O_6$: C, 57.06 ; H, 3.48; N, 6.05. Found: C, 56.98; H, 3.48; N, 5.93

N,N′-Bis[4-[[1-(2-ethyl)piperidine]oxy]salicylidene]-4-methylester-1,2-phenylenediamine-nickel(II) (***9***). A suspension of **3** (0.132 g, 0.3 mmol), 1-(2-chloroethyl)piperidine hydrochloride (0.276 g, 1.5 mmol), and K_2CO_3 (0.332 g, 2.4 mmol) in dry DMF (30 mL) was heated at 90 °C overnight. After 24 h of stirring, the excess salts were removed by filtration and the DMF evaporated under reduced pressure. The resulting dark-red solid was recrystallized with DCM:*n*-pentane (1:5) to give **9** as an orange solid. Yield: 0.042 g, 20.2%. ^{1}H NMR (400 MHz, $CDCl_3$): δ 1.48 (br m, 4H, piperidine H), 1.65−1.64 (br m, 8H, piperidine H), 2.52 (s, 8H, piperidine H), 2.81 (t, $^3J_{HH}$ = 5.6 Hz, 4H, $-CH_2N-$), 3.98 (s, 3H, CH_3OCO-), 4.15 (t, $^3J_{HH}$ = 5.6, 4H, $-CH_2O-$), 6.40−6.37 (m, 2H, ArH,), 6.63−6.62 (m, 2H, ArH), 7.22 (d, $^3J_{HH}$ = 8.8 Hz, 1 H, ArH), 7.27 (d, $^3J_{HH}$ = 8.8 Hz, 1H, ArH), 7.70(d, $^3J_{HH}$ = 8.8 Hz, 1H, ArH), 7.87 (dd, $^3J_{HH}$ = 8.8, $^4J_{HH}$ = 1.2 Hz, 1H, ArH), 8.12 (s, 1H, −CH═N−), 8.19 (s, 1H, −CH═N−), 8.34 (d, $^4J_{HH}$ = 1.2 Hz, 1H, ArH). ^{13}C NMR (400 MHz, $CDCl_3$): δ 24.2, 26.0, 52.5, 55.0, 57.6, 66.1, 103.0, 103.1, 109.5, 110.0, 114.1, 114.6, 114.8, 115.9, 127.4, 127.5, 132.5, 134.4, 142.6, 152.6, 153.0, 165.2, 165.7, 166.0, 168.1, 169.1. IR (cm^{-1}): 1714 (C═O), 1232 (HO−C═O), 1608 (C═N), 1122 (C−O), 2931 (CH_2), 2851 (CH−O), 1470 (C═C), 1504 (C═C). UV−vis ($CHCl_3$): λ_{max} = 394 nm (ε = 6.63 × 10^4 cm^{-1} M^{-1}), 320 nm (ε = 5.88 × 10^4 cm^{-1} M^{-1}). ESI-MS (M+) m/z calcd for $C_{36}H_{42}N_4NiO_6$ (M+), 685.4 amu; found, 685 amu Anal. Calcd for $C_{36}H_{42}N_4NiO_6$: C, 63.08; H,6.18; N, 8.17. Found: C, 62.98 ; H, 6.14; N, 8.18.

N,N′-Bis-4-(hydroxysalicylidene)4,5-difluorophenylenediamine-copper(II) (***5***). 1,2-Diamino-4,5-difluorobenzene (0.360 g, 2.5 mmol) and 2,4-dihydroxybenzaldehyde (0.699 g, 5.0 mmol) were reacted in absolute ethanol (50 mL) for 30 min at reflux. $Cu(OAc)_2{\cdot}H_2O$ (0.499 g, 5.0 mmol) was then added to this red mixture. The color of the solution changed immediately to dark-brown and a dark-green solid precipitated. The reaction was refluxed for a further 3 h. The dark-green precipitate was filtered and washed with ethanol (20 mL × 3), water (20 mL × 2), and diethyl ether (20 mL × 2) to afford **5** as a green solid. Yield: 0.968 g, 62.64%. ESI-MS (M+) m/z calcd for $C_{20}H_{12}CuF_2N_2O_4$ (M+), 445.86; found, 446. Anal. Calcd for $C_{20}H_{12}CuF_2N_2O_4$: C, 53.88; H, 2.71; N, 6.28. Found: C, 53.80; H, 2.62; N, 6.18.

N,N′-Bis[4-[[1-(2-ethyl)piperidine]oxy]salicylidene]-4,5-difluoro-1,2-phenylenediamine-copper(II) (***11***). A suspension of **5** (0.600 g, 1.4 mmol), 1-(2-chloroethyl)piperidine hydrochloride (1.240 g, 6.8 mmol), and K_2CO_3 (1.491 g, 10.8 mmol) in dry DMF (50 mL) was heated at 90 °C overnight. After this time, the excess salts were removed by filtration and the DMF evaporated under reduced pressure. The resulting dark-red solid was recrystallized twice with a DCM:*n*-pentane (1:5) mixture to give **11** as a green−yellow solid. Yield: 0.54 g, 60.1%. ESI-MS (M+) m/z calcd for $C_{34}H_{38}CuF_2N_4O_4$ (M+), 668.2 amu; found, 668 amu. Anal. Calcd for $C_{34}H_{38}CuF_2N_4O_4{\cdot}0.5DMF{\cdot}3H_2O$: C, 56.19 ; H, 6.31 ; N, 8.31. Found: C, 56.14 ; H, 5.98 ; N, 8.38.

N,N′-Bis-4-(hydroxysalicylidene)4-methylesterphenylenediamine-copper(II) (***6***). Methyl-3,4-diaminobenzoate (0.441 g, 2.5 mmol) and 2,4-dihydroxybenzaldehyde (0.699 g, 5.0 mmol) were reacted in absolute ethanol (40 mL) for 30 min at reflux. $Cu(OAc)_2{\cdot}H_2O$

dx.doi.org/10.1021/jm201140v | J. Med. Chem. 2012, 55, 209−222

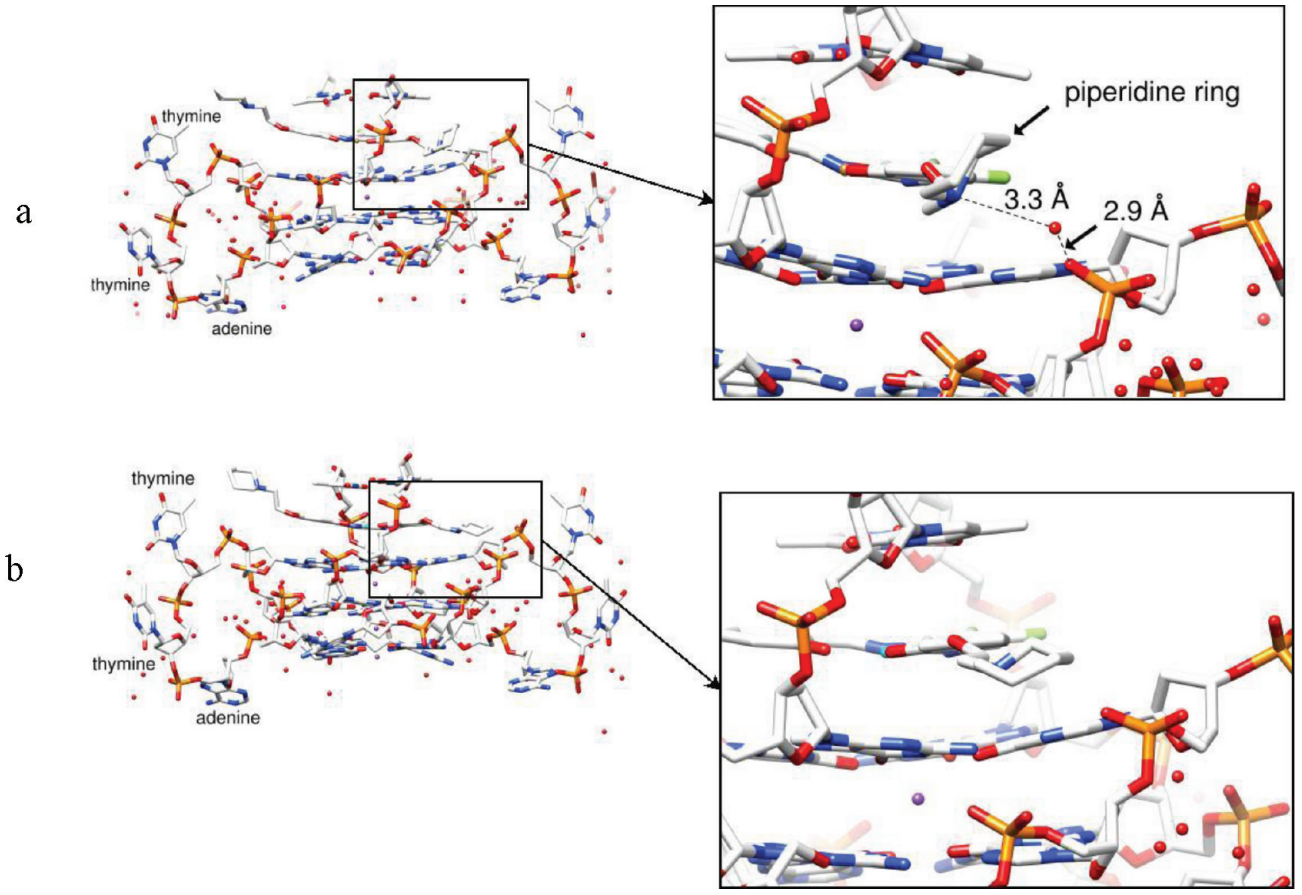

Figure 6. Views of the two side-chain piperidine rings (a) in the Cu^{2+} complex with the Cu^{2+} ion colored brown, (b) in the Ni^{2+} complex with the Ni^{2+} ion colored blue.

(0.499 g, 5.0 mmol) was then added to this red mixture. The color of the solution changed immediately to green−brown, and a green−brown solid precipitated. The reaction was refluxed for a further 3 h. The precipitate was filtered and washed with ethanol (20 mL × 3), water (20 mL × 2), and diethyl ether (20 mL × 2) to afford **6** as a green−brown solid. Yield: 1.29 g, 55.14%. ESI-MS (M+) m/z calcd for $C_{22}H_{16}CuN_2O_6$ (M+), 467.92 amu; found, 468 amu. Anal. Calcd for $C_{22}H_{16}CuN_2O_6$: C, 56.47; H, 3.45; N, 5.99. Found: C, 56.61; H, 3.50; N, 5.95.

*N,N′-Bis[4-[[1-(2-ethyl)piperidine]oxy]4-salicylidene]4-methyl-esterphenylenediamine-cooper (II) (**12**).* A suspension of **6** (0.234 g, 0.5 mmol), 1-(2-chloroethyl)piperidine hydrochloride (0.4603 g, 2.5 mmol), and K_2CO_3 (0.553 g, 4.0 mmol) in dry DMF (30 mL) was heated to 90 °C overnight. After this time, the excess salts were removed by filtration and the DMF evaporated under reduced pressure. The resulting dark-red solid was recrystallized with a DCM:*n*-pentane (1:5) mixture to give **12** as an green−yellow solid. Yield: 0.345 g, 58.33%. IR (cm^{-1}): 1716 (C═O), 1573 (C═N), 1121 (C−O), 2933 (CH_2), 2860 (CH−O). UV−vis ($CHCl_3$): λ_{max} = 407 nm. ESI-MS (M+) m/z calcd for $C_{36}H_{42}N_4CuO_6$ (M+), 690.29 amu; found, 690 amu. Anal. Calcd for $C_{36}H_{42}N_4CuO_6$: C, 62.64; H, 6.13; N, 8.12. Found: C, 62.56; H, 6.02; N, 8.16.

Fluorescent Intercalator Displacement (FID) Assay. The FID assay was performed on a Varian Cary Eclipse spectrometer following a reported procedure.[17] The oligonucleotide, 22-AG human telomeric (HTelo) DNA, 5′-AGGGTTAGGGTTAGGGTTAGGG-3′, used was purchased from Eurogentec SA. (UK).

UV−Vis Studies. The oligonucleotide, 22 AG human telomeric (Htelo) DNA, 5′-AGGGTTAGGG TTAGGGTTAGGG-3′, was purchased from Eurogentec SA. (UK). The oligonucleotide was dissolved in 10 mM Tris-HCl/100 mM KCl (pH 7.4) buffer to yield a 1 mM solution. The oligonucleotide was annealed by heating to 90 °C for 5 min and then cooled to room temperature overnight. Calf thymus DNA was purchased from Sigma-Aldrich and dissolved overnight in a 10 mM Tris-HCl/100 mM KCl (pH 7.4) buffer to yield a 2.76 mM solution. The test compounds were dissolved in a mixture of DMSO (95% by volume) and 1 mM HCl aqueous solution (5% by volume) to give 3.12−5.0 mM stock solutions. All solutions were stored at −20 °C and defrosted and diluted immediately before use. Prior to use, the compounds were diluted to 1 mM using DMSO. This was then further diluted using suitable buffer to the appropriate concentrations. The UV−vis spectra were recorded on a Perkin-Elmer Lambda 25 spectrometer. To determine the binding constants of the selected complexes with HTelo and CT-DNA, the complexes (20 μM) were titrated with concentrated solutions of DNA (HTelo, 1 mM; CT-DNA, 2.76 mM) in 10 mM Tris-HCl (pH 7.4)/100 mM KCl buffer. A 1 cm path-length quartz cuvette was used to carry out the measurements. The binding constants were obtained by fitting the data to a reciprocal plot of $D/\Delta\varepsilon_{ap}$ versus D using the following equation: $D/\Delta\varepsilon_{ap} = D/\Delta\varepsilon + 1/(\Delta\varepsilon \times K)$, where the concentration of DNA is expressed in terms of base pairs (determined by measuring the absorption at 260 nm and the appropriate extinction coefficients), the apparent molar extinction coefficient $\varepsilon_a = A_{observed}/[\text{Complex}]$, $\Delta\varepsilon_{ap} = [\varepsilon_a - \varepsilon_f]$, and $\Delta\varepsilon = [\varepsilon_b - \varepsilon_f]$. ε_b is the extinction coefficient of the DNA bound complex, and ε_f is the extinction coefficient of the free complex.

Circular Dichroism (CD) Studies. The 22-mer sequence HTelo oligonucleotide, 5′-d(AGGGTTAGGGTTAGGGTTAGGG)-3′, was purchased from Eurogentec SA. (U.K.). The oligonucleotide was dissolved in Milli Q water to yield a 100 μM stock solution. This was then diluted using 50 mM Tris-HCl/150 mM KCl buffer (pH 7.4) or Trizma hydrochloride buffer (0.1M, pH 7.4) to 20 μM. Prior to use in the CD assay, the DNA solution was either annealed or remained nonannealed. The DNA solution was annealed by heating the solution to 90 °C for 5 min and then by cooling to room temperature

dx.doi.org/10.1021/jm201140v | J. Med. Chem. 2012, 55, 209−222

overnight. The test compounds were dissolved in a mixture of DMSO (95% by volume) and 1 mM HCl (5% by volume) to give 3.12–5.0 mM stock solutions. All solutions were stored at −20 °C and defrosted and diluted immediately before use. Prior to use, the compounds were diluted to 1 mM using DMSO. This was then further diluted using suitable buffer to the appropriate concentrations. The CD spectra were recorded in a strain-free 10 mm × 2 mm rectangular cell path length cuvette. The data was obtained on an Applied Photophysics Ltd. Chirascan spectrometer. The CD spectra were measured in the wavelength region of 700–180 nm with the following parameters: bandwidth, 1 nm; spectral range, 230–600 nm; step-size, 0.5 nm; time-pep-point, 1.5 s. The CD spectra were collected and analyzed using the Chirascan and Chirascan Viewer software, respectively. The following CD spectra were recorded: (1) CD spectra of annealed HTelo DNA (10 μM) in 50 mM tris-HCl and 150 mM KCl buffer (pH 7.4), with 0–5 equiv of test compounds, (2) CD spectra of HTelo DNA (10 μM) in Trizma hydrochloride buffer (0.1M, pH 7.4), annealed with 0–6 equiv of the test compounds, (3) CD spectra of nonannealed HTelo DNA (10 μM) in Trizma hydrochloride buffer (0.1 M, pH 7.4), with 0–6 equiv of the test compounds. FRET experiments were performed using protocols previously described by us.[6,7,11]

Modified Telomerase Repeat Amplification Protocol (TRAP-LIG).[19] A 10 mM stock solution of each ligand was made in 100% DMSO followed by a further dilution (1 mM) in distilled water with 1% HCl. The 1 mM stock solution was prepared freshly before use. The TRAP assay was carried out in three steps with an initial primer elongation step by telomerase, a subsequent removal of the primer bound ligand, and a final PCR amplification of the telomerase products. The first step of the TRAP assay was carried out by preparing a master mix containing the TS forward primer (0.1 μg; 5′-d(AATCCGTCGAGCAGAGTT)-3′, TRAP buffer (20 mM Tris-HCl [pH 8.3], 68 mM KCl, 1.5 mM $MgCl_2$, 1 mM EGTA, 0.05% v/v Tween-20), bovine serum albumin (0.05 μg), and dNTPs (125 μM each), protein extract (500 μg/sample) diluted in lysis buffer (10 mM Tris-HCl, pH 7.5, 1 mM $MgCl_2$, 1 mM EGTA, 0.5% CHAPS, 10% glycerol, 5 mM β-mercaptoethanol, 0.1 mM AEBSF).

The PCR master mix was added to tubes containing freshly prepared compounds at various concentrations and to the negative control containing no drug. The initial elongation step was carried out for 10 min at 30 °C, followed by at 94 °C for 5 min and a final maintenance of the mixture at 20 °C. To purify the elongated product and to remove the bound ligands, the QIAquick nucleotide purification kit (Qiagen) was used according to manufacturer's instructions. The kit is especially designed for the purification of both double- and single-stranded oligonucleotides from 17 bases in length. The kit employs a high salt concentration buffer to bind the negatively charged oligonucleotides to the positively charged spin-tube membrane through centrifugation. An ethanol based buffer is then used to wash any impurities away before elution of the DNA using a low salt concentration solution. This was substituted with PCR-grade water in our experiments. The purified extended samples were then subject to PCR amplification. For this, a second PCR master mix was prepared consisting of ACX reverse primer (1 μM; 5′-d(GCGCGG[CTTACC]$_3$-CTAACC)-3′), TS forward primer (0.1 μg; 5′-d(AATCCGTCGA-GCAGAGTT)-3′), TRAP buffer, BSA (5 μg), 0.5 mM dNTPs, and 2U of taq polymerase. An aliquot of 10 μL of the master mix was added to the purified telomerase extended samples and amplified at: 35 cycles of 94 °C for 30 s, 61 °C for 1 min, and 72 °C for 1 min. samples were separated on a 12% PAGE and visualized with SYBR green staining. Fluorescence from drug samples was normalized against a positive control containing protein only. All samples were corrected for background by subtracting the fluorescence reading of negative controls.

Sulforhodamine B Short-Term Cytotoxicity Assay. Human cancer cell lines, breast (MCF7), lung (A549), pancreatic (MIA-Pa-Ca-2, HPAC), renal (RCC4, RCC4-VHL, 786–0), and normal human lung fibroblast lines (WI-38), were all purchased from American Type Cell Culture (ATCC). Cell lines were maintained in appropriate medium supplemented with 10% fetal bovine serum (Invitrogen, UK), 2 mM L-glutamine (Invitrogen, Netherlands), and other components as specified by the suppliers. All cell lines were maintained at 37 °C, 5% CO_2, and routinely passaged. Short-term growth inhibition was measured using the SRB assay as described previously. Briefly, cells were seeded at appropriate densities into the wells of 96 well-plates in their corresponding medium and incubated overnight to allow the cells to attach. Subsequently cells were exposed to freshly made solutions of drugs and incubated for a further 96 h. Following this, the cells were fixed with ice-cold trichloaceticacid (TCA) (10%, w/v) for 30 min and stained with 0.4% SRB dissolved in 1% acetic acid for 15 min. All incubations were carried out at room temperature except for TCA fixation, which was at 4 °C. The IC_{50} value, the concentration required to inhibit cell growth by 50%, was determined from the mean absorbance at 540 nm for each drug concentration expressed as a percentage of the control untreated well absorbance.

Crystallization Experiments. The HPLC-purified human telomeric DNA sequences were purchased from DNA Technology A/S (Denmark) and used without further purification. Both sequences, native d(AGGGTTAGGGTT) and the brominated d(AGGGT^{Br}-UAGGGTT) (where ^{Br}U is 5-bromo-2′-deoxyuridine-5′-monophosphate), were annealed at 3 mM (quadruplex concentration) before use by incubation in a heating block at 80 °C for 15 min in 20 mM potassium cacodylate buffer at pH 7.0 and left overnight to cool gradually to room temperature. Stock solutions were prepared for each of the metal-containing ligands by dissolving in 100% DMSO (dimethyl sulfoxide) at a concentration of 20 mM. The stock solutions were kept at −20 °C. The relevant stock solution was thawed immediately prior to setting up the crystallization drops. The hanging-drop vapor-diffusion method was used. The Crystalgen 24-well SuperClear Plates (Jena Bioscience) and 22 mm circular siliconized glass coverslips (Molecular Dimensions) were used in the setup. In both instances, crystals grew as yellow plates after 3 weeks at 20 °C.

Crystals of the **11**-quadruplex complex grew in the following initial crystallization conditions: 0.6 mM quadruplex DNA, 0.6 mM ligand, 0.4% (w/v) PEG 2000, 20 mM potassium cacodylate buffer at pH 7.0. This was equilibrated against a reservoir well solution of 60% (w/v) PEG 2000. Prior to mounting the crystals, they were cryoprotected in a solution containing 140 mM of each of potassium chloride, sodium chloride, and lithium sulfate, as well as 12.5% (w/v) PEG 2000 and 25% glycerol.

Crystals of the **8**-quadruplex complex grew from a 3 μL drop containing 1.25 mM quadruplex DNA, 1.25 mM ligand, 0.83% PEG (w/v) 10 000, 16.7 mM potassium chloride, 16.7 mM sodium chloride, 16.7 mM lithium sulfate, and 20 mM potassium cacodylate buffer at pH 7.0. This was equilibrated against a reservoir well solution of 50% (w/v) PEG 10,000. No cryoprotection agent was required.

Data Collection, Processing, Structure Solution, Verification, and Crystallographic Refinement. Data were collected for each of the cocrystals of **8**-quadruplex, **11**-quadruplex, and **13**-quadruplex on beamline ID IO3 at the Diamond Light Source synchrotron. The structure of the **11**-quadruplex was determined using experimental phases obtained using data collected to a resolution of 2.3 Å at three wavelengths in a multiple anomalous dispersion (MAD) experiment using the bromine atom as the anomalous scatterer. A single-flash frozen crystal was used at 105 K. Diffraction data was processed and scaled with the MOSFLM[23] and SCALA20 software packages. The space group was determined at this point as *C*222. The data set collected at the peak wavelength 0.92060 Å was reprocessed with the XDS software package[24] and used for high-resolution refinement. The structure of the **11**-quadruplex complex was solved by a combination of MAD and MR techniques. The position of the bromine atom was initially determined by MAD phasing using the SHELXC/D/E[25−27]suite of programs utilizing the bromine *K*-absorption edge, although otherwise the MAD maps were uninterpretable in terms of a discrete quadruplex structure. The EPMR program[28] was then used to solve the rest of the structure by molecular replacement using a partial model formed of the G-quartets only extracted from the native parallel quadruplex structure (PDB ID 1K8P).[29] Electron density maps were calculated for each of the solutions produced by EPMR, but only one solution confirmed the position of the bromine atom from the MAD phasing and this resulted in interpretable maps. The loops were built into subsequent electron density maps, which then revealed a

volume similar in shape to the ligand clearly visible along the 2-fold symmetry axis, and the ligand was fitted to this with a 2-fold disordered model. The crystal structure coordinates for the complex closely related to **11** were imported from the Cambridge Structural Database (CSD) (reference code LOQKUY)[15] and used to generate restraints for crystallographic refinement with the Refmac program.[30] Water molecules were located by hand in subsequent maps. The position of the 3′ terminal thymidine nucleotide could not be unambiguously assigned in either structure and has not been included in the deposited coordinates.

The structure of the **8**-quadruplex complex was determined by molecular replacement (MR) using the program PHASER[31] and the **11**-quadruplex structure as a starting point. Similarly, the electron density maps revealed a volume similar in shape to two discrete positions for the disordered ligand, which was fitted accordingly, followed by the location of water molecules. The atomic coordinates and structure factors were deposited in the Protein Data Bank (PDB) database with accession codes 3QSC and 3QSF. Programs COOT v. 0.6.1,[32] CHIMERA v.1.5.230[33] and PyMOL v. 0.99rc6 (Schrodinger Inc.)[34] were used in model visualization and image production. Programs from the CCP4 suite[35] were used as appropriate.

■ ASSOCIATED CONTENT

Ⓢ Supporting Information

Synthetic protocols, crystallographic data, fluorescent intercalator displacement (FID) assays, FRET melting curves, and UV−VIS spectra and reciprocal plots of D/ε_{ap} versus D. This material is available free of charge via the Internet at http://pubs.acs.org.

Accession Codes

Protein Data Bank (PDB) accession codes for the structures reported in this work are: 3QSC and 3QSF.

■ AUTHOR INFORMATION

Corresponding Author

*For S.N.: phone, 44 207 753 5969; fax, 44 207 753 5970; E-mail, stephen.neidle@pharmacy.ac.uk. For R.V.: phone, 44 2075941967; E-mail, r.vilar@imperial.ac.uk.

Author Contributions

[§]Nancy H. Campbell and Nurul H. Abd Karim contributed equally to this work.

■ ACKNOWLEDGMENTS

We are grateful to Cancer Research UK (programme grant no. C129/A4489 to S.N.), EPSRC (Leadership Fellowship for R.V.; grant no. EP/H005285/1), and the Malaysian Government for a studentship (N.H.A.K.). We are grateful to the Diamond Light Source for access to beamline ID IO3.

■ ABBREVIATIONS USED

OAc, acetyl; FID, fluorescent intercalator displacement; FRET, fluorescence resonance energy transfer; HTelo, human telomeric; TRAP, telomerase repeat amplification protocol; CT, calf thymus; MAD, multiwavelength anomalous dispersion (MAD) phasing method; MR, molecular replacement; CD, circular dichroism

■ REFERENCES

(1) de Lange, T. Shelterin: the protein complex that shapes and safeguards human telomeres. *Genes Dev.* **2005**, *19*, 2100−2110. de Lange, T. How Shelterin solves the telomere end-replication problem. *Cold Spring Harbor Symp. Quant. Biol.* **2010**, *75*, 167−177.

(2) Oganesian, L.; Bryan, T. M. Physiological relevance of telomeric G-quadruplex formation: a potential drug target. *BioEssays* **2007**, *29*, 155−165. Mason, M.; Schuller, A. P.; Skordalakes, E. Telomerase structure function. *Curr. Opin. Struct. Biol.* **2010**, *21*, 1−9. Shay, J. W.; Wright, W. E. Telomerase: a target for cancer therapeutics. *Cancer Cell* **2010**, *2*, 257−265.

(3) Zahler, A. M.; Williamson, J. R.; Cech, T. R.; Prescott, D. M. Inhibition of telomerase by G-quartet DNA structures. *Nature* **1991**, *350*, 718−750. Sun, D.; Thompson, B.; Cathers, B. E.; Salazar, M.; Kerwin, S. M.; Trent, J. O.; Jenkins, T. C.; Neidle, S.; Hurley, L. H. Inhibition of human telomerase by a G-quadruplex-interactive compound. *J. Med. Chem.* **1997**, *40*, 2113−2116. De Cian, A..; Lacroix, L..; Douarre, C..; Temime-Smaali, N.; Trentesaux, C.; Riou, J.-F.; Mergny, J.-L. Targeting telomeres and telomerase. *Biochimie* **2008**, *90*, 131−155. Wang, Q.; Liu, J.-Q.; Chen, Z.; Zheng, K.-W.; Chen, C.-Y.; Hao, Y.-H.; Tan, Z. G-quadruplex formation at the 3′ end of telomere DNA inhibits its extension by telomerase, polymerase and unwinding by helicase. *Nucleic Acids Res.* **2011**, *39*, 6229−6237.

(4) Monchaud, D.; Teulade-Fichou, M.-P. A hitchhiker's guide to G-quadruplex ligands. *Org. Biomol. Chem.* **2008**, *6*, 627−636.

(5) Arola, A.; Vilar, R. Stabilisation of G-quadruplex DNA by small molecules. *Current Top. Med. Chem.* **2008**, *8*, 1405−1415.

(6) Reed, J. E.; Arnal, A. A.; Neidle, S.; Vilar, R. Stabilization of G-quadruplex DNA and inhibition of telomerase activity by square-planar nickel(II) complexes. *J. Am. Chem. Soc.* **2006**, *128*, 5992−5993.

(7) Reed, J. E.; Neidle, S.; Vilar, R. Stabilisation of human telomeric quadruplex DNA and inhibition of telomerase by a platinum−phenanthroline complex. *Chem. Commun.* **2007**, 4366−4368.

(8) Shi, D.-F.; Wheelhouse, R. T.; Sun, D.; Hurley, L. H. Quadruplex-interactive agents as telomerase inhibitors: synthesis of porphyrins and structure−activity relationship for the inhibition of telomerase. *J. Med. Chem.* **2001**, *44*, 4509−4523.

(9) Bertrand, H.; Monchaud, D.; De Cian, A.; Guillot, R.; Mergny, J.-L.; Teulade-Fichou, M.-P. The importance of metal geometry in the recognition of G-quadruplex-DNA by metal−terpyridine complexes. *Org. Biomol. Chem.* **2007**, *5*, 2555−2559.

(10) Georgiades, S. N.; Abd Karim, N. H.; Suntharalingam, K.; Vilar, R. Interaction of metal complexes with G-quadruplex DNA. *Angew. Chem., Int. Ed.* **2010**, *49*, 4020−4034.

(11) Reed, J. E.; White, A. J. P.; Neidle, S.; Vilar, R. Effect of metal coordination on the interaction of substituted phenanthroline and pyridine ligands with quadruplex DNA. *Dalton Trans.* **2009**, *14*, 2558−2568.

(12) Suntharalingam, K.; Gupta, D.; Sanz Miguel, P. J.; Lippert, B.; Vilar, R. Synthesis, structural characterisation and quadruplex DNA binding studies of a new gold(III) pyrazolylpyridine complex. *Chem.—Eur. J.* **2010**, *16*, 3613−3616.

(13) Suntharalingam, K.; White, A. J. P.; Vilar, R. Synthesis, structural characterization, and quadruplex DNA binding studies of platinum(II)−terpyridine complexes. *Inorg. Chem.* **2009**, *48*, 9427−9435.

(14) Suntharalingam, K.; White, A. J. P.; Vilar, R. Two metals are better than one: investigations on the interactions between dinuclear metal complexes and quadruplex DNA. *Inorg. Chem.* **2010**, *49*, 8371−8380.

(15) Arola-Arnal, A.; Benet-Buchholz, J.; Neidle, S.; Vilar, R. Effects of metal coordination geometry on stabilization of human telomeric quadruplex DNA by square-planar and square-pyramidal metal complexes. *Inorg. Chem.* **2008**, *47*, 11910−11919.

(16) Wu, P.; Ma, D.-L.; Leung, C.-H.; Yan, S.-C.; Zhu, N.; Abagyan, R.; Che, C.-M. Stabilization of G-quadruplex DNA with platinum(II) Schiff base complexes: luminescent probe and down-regulation of c-myc oncogene expression. *Chem.—Eur. J.* **2009**, *15*, 13008−13021.

(17) Monchaud, D.; Allain, C.; Teulade-Fichou, M.-P. Development of a fluorescent intercalator displacement assay (G4-FID) for establishing quadruplex−DNA affinity and selectivity of putative ligands. *Biorg. Med. Chem. Let.* **2006**, *16*, 4842−4845.

(18) Kieltyka, R.; Fakhoury, J.; Moitessier, N.; Sleiman, H. F. Platinum phenanthroimidazole complexes as G-quadruplex DNA selective binders. *Chem.—Eur. J.* **2008**, *14*, 1145−1154.

(19) Reed, J.; Gunaratnam, M.; Beltran, M.; Reszka, A. P.; Vilar, R.; Neidle, S. TRAP-LIG, a modified telomere repeat amplification protocol assay to quantitate telomerase inhibition by small molecules. *Anal. Biochem.* **2008**, *380*, 99−105.
(20) (a) Neidle, S.; Parkinson, G. N. Quadruplex DNA crystal structures and drug design. *Biochimie* **2008**, *90*, 1184−1196. (b) Campbell, N. H.; Parkinson, G. N.; Reszka, A. P.; Neidle, S. Structural basis of DNA quadruplex recognition by an acridine drug. *J. Am. Chem. Soc.* **2008**, *130*, 6722−6724. (c) Parkinson, G. N.; Cuenca, F.; Neidle, S. Topology conservation and loop flexibility in quadruplex−drug recognition: crystal structures of inter- and intramolecular telomeric DNA quadruplex−drug complexes. *J. Mol. Biol.* **2008**, *381*, 1145−1156. (d) Collie, G. W.; Sparapani, S.; Parkinson, G. N.; Neidle, S. Structural basis of telomeric RNA quadruplex−acridine ligand recognition. *J. Am. Chem. Soc.* **2011**, *133*, 2721−2728.
(21) Balasubramanian, S.; Hurley, L. H.; Neidle, S. Targeting G-quadruplexes in gene promoters: a novel anticancer strategy? *Nature Rev. Drug Discovery* **2011**, *10*, 261−275.
(22) Campbell, N. H.; Patel, M.; Tofa, A, B.; Ghosh, R.; Parkinson, G. N.; Neidle, S. Selectivity in ligand recognition of G-quadruplex loops. *Biochemistry* **2009**, *48*, 1675−1680.
(23) Leslie, A. G. W. Recent changes to the MOSFLM package for processing film and image plate data. *Joint CCP4 + ESF-EAMCB Newsletter on Protein Crystallography* **1992**, 26.
(24) Kabsch, W. Software XDS for image rotation, recognition and crystal symmetry assignment. *Acta Crystallogr., Sect. D: Biol. Crystallogr.* **2010**, *66*, 125−132.
(25) Beck, T.; Gruene, T.; Sheldrick, G. M. The magic triangle goes MAD: experimental phasing with a bromine derivative. *Acta Crystallogr., Sect. D: Biol. Crystallogr.* **2010**, *66*, 374−380.
(26) Sheldrick, G. M. A short history of SHELX. *Acta Crystallogr., Sect. A: Found. Crystallogr.* **2008**, *64*, 112−122.
(27) Sheldrick, G. M. Experimental phasing with SHELXC/D/E: combining chain tracing with density modification. *Acta Crystallogr., Sect. D: Biol. Crystallogr.* **2010**, *66*, 479−485.
(28) Kissinger, C. R.; Gehlhaar, D. K.; Smith, B. A.; Bouzida, D. Molecular replacement by evolutionary search. *Acta Crystallogr., Sect. D: Biol. Crystallogr.* **2001**, *57*, 1474−1479.
(29) Parkinson, G. N.; Lee, M. P. H; Neidle, S. Crystal structure of parallel quadruplexes from human telomeric DNA. *Nature* **2002**, *417*, 876−880.
(30) Vagin, A. A.; Steiner, R. A.; Lebedev, A. A.; Potterton, L.; McNicholas, S.; Long, F.; Murshudov, G. N. REFMAC5 dictionary: organization of prior chemical knowledge and guidelines for its use. *Acta Crystallogr., Sect. D: Biol. Crystallogr.* **2004**, *60*, 2184−2195.
(31) McCoy, A. J.; Grosse-Kunstleve, R. W.; Adams, P. D.; Winn, M. D.; Storoni, L. C.; Read, R. J. Phaser crystallographic software. *J. Appl. Crystallogr.* **2007**, *40*, 658−674.
(32) Emsley, P.; Lohkamp, B.; Scott, W. G.; Cowtan, K. Features and development of Coot. *Acta Crystallogr., Sect. D: Biol. Crystallogr.* **2010**, *66*, 486−501.
(33) Pettersen, E. F.; Goddard, T. D.; Huang, C. C.; Couch, G. S.; Greenblatt, D. M.; Meng, E. C.; Ferrin, T. E. UCSF Chimera—a visualization system for exploratory research and analysis. *J. Comput. Chem.* **2004**, *25*, 1605−1612.
(34) DeLano, W. L. *The PyMOL Molecular Graphics System*; DeLano Scientific LLC: Palo Alto, CA, 2008; http://www.pymol.org
(35) The CCP4 suite: programs for protein crystallography. *Acta Crystallogr., Sect. D: Biol. Crystallogr.* **1994**, *50*, 760−763.

■ NOTE ADDED AFTER ASAP PUBLICATION

After this paper was published online December 13, 2011, corrections were made to the caption of Figure 2. The corrected version was published December 15, 2011.